Nuclear Instruments and Methods in Physics Research A ∎ (∎∎∎∎) ∎∎∎–∎∎∎

Contents lists available at ScienceDirect

Nuclear Instruments and Methods in Physics Research A

journal homepage: www.elsevier.com/locate/nima

Characterisation and magnetic field properties of multianode photomultiplier tubes

Q1 Stephan Eisenhardt, Haofei Luo, Adam Morris, Matthew Needham, Josh Neill

University of Edinburgh, School of Physics & Astronomy, Edinburgh EH9 3JZ, UK

On behalf of the LHCb RICH Collaboration

A R T I C L E I N F O

Keywords:
Multianode photomultiplier tubes
Cherenkov counters
LHCb RICH

A B S T R A C T

We report on studies of the Hamamatsu model R11265 Multianode Photomultiplier as part of the effort to qualify their use in the upgrade of the LHCb Ring Imaging Cherenkov Detectors. Comparisons with the known model R7600 are also made. Of particular interest is the behaviour of the MaPMT in magnetic fields comparable to the residual fringe field of the LHCb bending magnet ranging up to 25 Gauss.

1. Introduction

The upgrade of the LHCb experiment [1] will introduce 40 MHz readout to all sub-detectors. All on-detector readout electronics, currently limited to a readout rate of 1 MHz, will be replaced. Consequently, the Hybrid Photon Detectors [2] currently used in the LHCb Ring Imaging Cherenkov Detectors (RICH) [3] need to be replaced together with the readout chip [4] that is embedded in the tubes. The baseline for the photon detector replacement is the Multianode Photomultiplier R11265 from Hamamatsu [5]. For operation in LHCb the behaviour in magnetic fields is critical. The photon detectors are located within the fringe field of the LHCb dipole magnet. Even with global shielding of the photon detector boxes they are subjected to residual fields of up to 25 Gauss and may need further individual shielding.

2. MaPMT

We characterise the latest generation of MaPMT, Hamamatsu R11265, and compare to the previous generation, R7600. Both provide single photon sensitivity in the range 200–600 nm, high Quantum Efficiency of above 25% at 370 nm and a spatial resolution of better than 3 mm matching our needs. Compared to the R7600 the geometry of the R11265 has been significantly changed. This is illustrated in Fig. 1. The total active area fraction increased to 77%, compared to 50% provided by the R7600. Therefore, the R11265 may be used without lenses in LHCb RICH and still maintain a large enough photon yield. However, the redesign of the geometry also appears to cause the R11265 to be more sensitive to magnetic fields than previously established for the R7600. Notably the top and bottom row (pixels 1–8 and 57–64 in the pixel numbering scheme) turn out to be affected the most by magnetic fields. This correlates with these pixels featuring smaller pixel sizes, which are nearly 20% shorter in the direction of the entry slits, i.e. the *y*-direction of the local coordinate system, providing the room to distribute the potentials to the dynode structures. The R11265 shows better separation of the single photoelectron signal from noise (pedestal) than the R7600, which can be seen when comparing the typical signal spectra from both models, given in Figs. 2 and 3, respectively. The fits of the 1- and 2-photon contributions as well as for the photoelectron rate are modelled by Poisson distributions. Higher orders are treated with Gaussian distributions. The spectrum for the R11265 was taken at a high voltage of 800 V, i.e. 200 V below the nominal bias of 1000 V. Already at this bias the R11265 typically shows a clear valley between pedestal and 1-photoelectron contribution. Increasing the bias separates the signal further from the pedestal. The spectrum for the R7600 was taken at its nominal high voltage setting of 900 V.

Since the R11265 is clearly preferred for the larger active area and better signal-to-noise behaviour it is necessary to understand well its performance limitations in a magnetic field to evaluate its use in the LHCb RICH detectors.

3. Test setup

We use pulsed LED light with a wavelength of 470 nm and a pulse width of 15 ns to illuminate the MaPMT. We deliver the light

---

E-mail address: S.Eisenhardt@ed.ac.uk (S. Eisenhardt).

http://dx.doi.org/10.1016/j.nima.2014.05.036
0168-9002/© 2014 Published by Elsevier B.V.

Please cite this article as: S. Eisenhardt, et al., Nuclear Instruments & Methods in Physics Research A (2014), http://dx.doi.org/10.1016/j.nima.2014.05.036

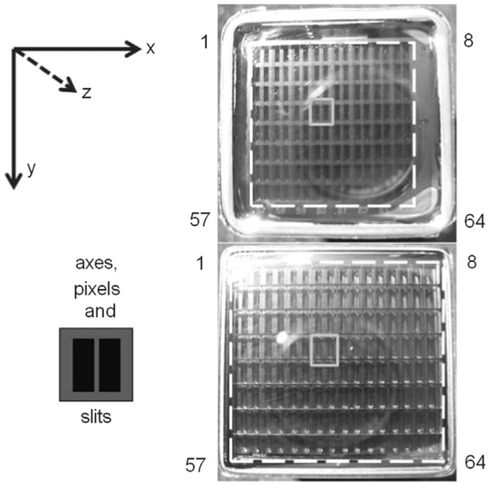

Fig. 1. Geometry of MaPMTs: entry window of R7600 (top) and R11265 (bottom); also indicated are: the total active area (approx. $(18.0\ \text{mm})^2$ and $(26.0\ \text{mm})^2$), the single pixel area (approximately $((2.3\ \text{mm})^2$ and $(2.9\ \text{mm})^2)$, the orientation of the entry slits per pixel, the pixel numbering scheme and the local coordinate system.

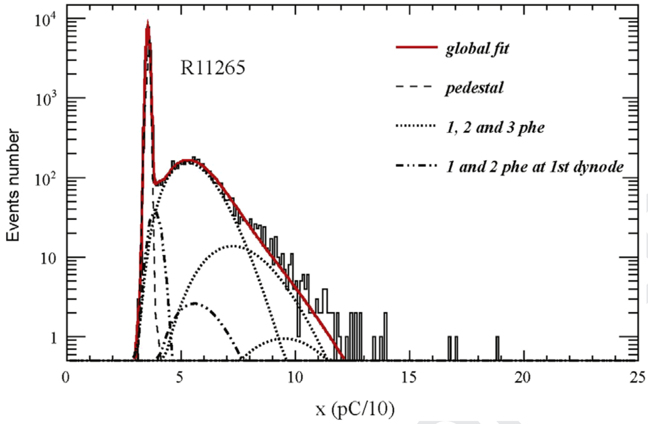

Fig. 2. Typical single photoelectron spectrum of a single pixel of a R11265, recored at HV = 800 V, with Poisson fit for the photoelectron signal.

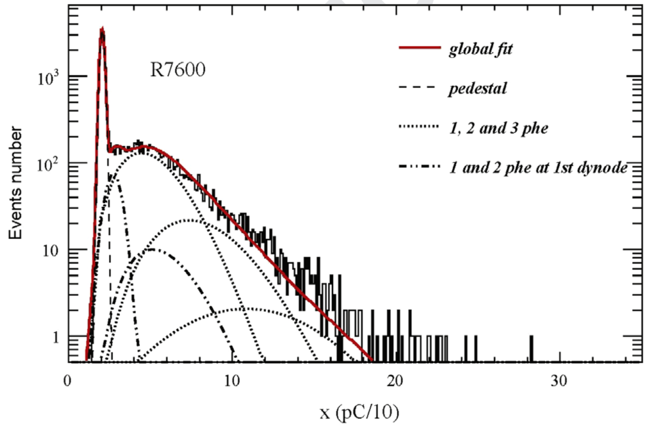

Fig. 3. Typical single photoelectron spectrum of a single pixel of a R7600, recored at HV = 900 V, with Poisson fit for the photoelectron signal.

via a light guiding fibre and focus it to a spot size of ~0.1 mm using a graded index lens. The fibre end and lens are mounted on a xy-stage and illuminate one pixel at a time. This setup also allows to use Helmholtz coils which can deliver a magnetic field of up to 30 Gauss (3 mT) to the MaPMT. The entire setup is encapsulated in a dark and electrically shielded box.

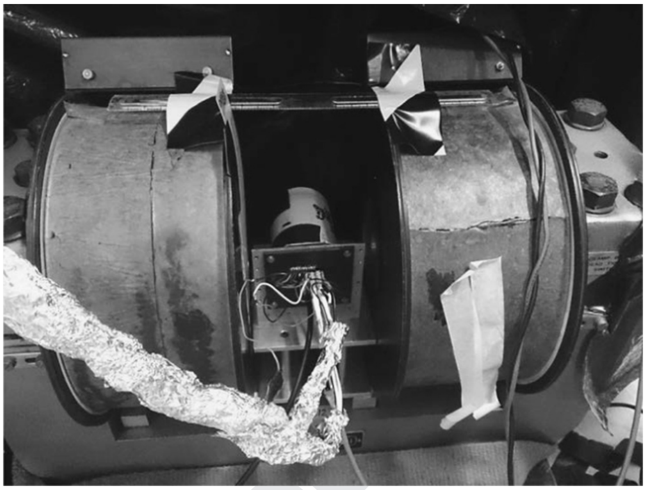

Fig. 4. Setup with small MaPMT enclosure mounted between pole shoes of stronger magnet.

Alternatively we can mount the MaPMT in a small dark cylinder, which fits into the opening of a stronger magnet, delivering fields of up to 300 Gauss (30 mT). The latter setup is shown in Fig. 4. In this small cylinder the pulsed light is delivered by the light guide entering from the back and the light reflecting diffusely off white paper fitting out the front part of the cylinder. This results in a fairly homogeneous illumination of the whole active area of the MaPMT. The intensity of the light source can be regulated to always produce spectra which are dominated by single photoelectron signals, as shown in Figs. 2 and 3. The adjustment is done online observing the single photoelectron pulses on an oscilloscope and quantified offline using the fit to a recorded signal spectrum. The intensity of the light source is sufficiently stable to neglect any variations. To match the dynamic range of the subsequent electronics the charge pulses emerging from the MaPMT are amplified by a factor × 100, using a sequence of two linear amplifiers per channel, each with a bandwidth of 350 MHz and individual gains of × 10. The amplified charge signals are recorded by CAEN V792 charge integrating ADCs, using a gate width of ~35 ns. Due to the limited number of available amplifiers only 16 MaPMT channels are recorded at the same time. Two connectors with a 4×2-pixel layout are used to connect to the 8×8 pin-grid-array at the base of the MaPMT. These connectors can be placed arbitrarily on the array, but for many tests it is convenient to test the four quadrants of the MaPMT in sequence. The unconnected pixels always are properly grounded to prevent internal charge-up of the anodes.

4. MaPMT characterisation and response to magnetic fields

Fig. 5 shows the signal gain across the array of pixels for the R11265 and R7600, exhibiting significantly different patterns. The R11265 has high gain in top and bottom row (pixels 1–8 and 57–64) and minimum gain in the centre, while the R7600 shows opposite behaviour. Fig. 6 shows the correlation between charge pulses of two adjacent pixels, of which only one is illuminated. Each data point represents the recorded charges for one light pulse without external magnetic field. The amount of charge found in a neighbouring channel due to cross-talk is expected to be linearly related to the charge produced in the illuminated pixel. Thus, the fitted slope of the distribution is a measure of the strength of the cross-talk. In Fig. 6 after the pedestal cut about 2000 data points are left, predominantly from single photon events. The few events with larger signal content nicely demonstrate the linearity.

Please cite this article as: S. Eisenhardt, et al., Nuclear Instruments & Methods in Physics Research A (2014), http://dx.doi.org/10.1016/j.nima.2014.05.036